ISSN 1674-1056
http://cpb.iphy.ac.cn
http://iopscience.iop.org/cpb
中国物理 B
Chinese Physics
中国物理
Chinese Physics B

Phase-field study of spinodal decomposition under effect of grain boundary

Ying-Yuan Deng(邓英远), Can Guo(郭灿), Jin-Cheng Wang(王锦程), Qian Liu(刘倩), Yu-Ping Zhao(赵玉平), and Qing Yang(杨卿)

Citation: Chin. Phys. B, 2021, 30 (**8**): 088101. DOI: 10.1088/1674-1056/abea9b
Journal homepage: http://cpb.iphy.ac.cn; http://iopscience.iop.org/cpb

What follows is a list of articles you may be interested in

Modeling of microporosity formation and hydrogen concentration evolution during solidification of an Al-Si alloy

Qingyu Zhang(张庆宇), Dongke Sun(孙东科), Shunhu Zhang(章顺虎), Hui Wang(王辉), Mingfang Zhu(朱鸣芳)
Chin. Phys. B, 2020, 29 (**7**): 078104. DOI: 10.1088/1674-1056/ab8abb

Enhanced dielectric and optical properties of nanoscale barium hexaferrites for optoelectronics and high frequency application

J Mohammed, A B Suleiman, Tchouank Tekou Carol T, H Y Hafeez, Jyoti Sharma, Pradip K Maji, Sachin Godara Kumar, A K Srivastava
Chin. Phys. B, 2018, 27 (**12**): 128104. DOI: 10.1088/1674-1056/27/12/128104

Material microstructures analyzed by using gray level Co-occurrence matrices

Yansu Hu(胡延苏), Zhijun Wang(王志军), Xiaoguang Fan(樊晓光), Junjie Li(李俊杰), Ang Gao(高昂)
Chin. Phys. B, 2017, 26 (**9**): 098104. DOI: 10.1088/1674-1056/26/9/098104

Cyclic stress induced phase transformation insuper-bainitic microstructure

Wencui Xiu(修文翠), Ying Han(韩英), Cheng Liu(刘澄), Hua Wu(吴化), Yunxu Liu(刘云旭)
Chin. Phys. B, 2017, 26 (**3**): 038101. DOI: 10.1088/1674-1056/26/3/038101

Improved thermoelectric property of cation-substituted $CaMnO_3$

Pradeep Kumar, Subhash C. Kashyap, Vijay Kumar Sharma, H. C. Gupta
Chin. Phys. B, 2015, 24 (**9**): 098101. DOI: 10.1088/1674-1056/24/9/098101

Phase-field study of spinodal decomposition under effect of grain boundary*

Ying-Yuan Deng(邓英远)[1], Can Guo(郭灿)[1,†], Jin-Cheng Wang(王锦程)[2], Qian Liu(刘倩)[1], Yu-Ping Zhao(赵玉平)[1], and Qing Yang(杨卿)[1]

[1] School of Materials Science and Engineering, Xi'an University of Technology, Xi'an 710048, China
[2] State Key Laboratory of Solidification Processing, Northwestern Polytechnical University, Xi'an 710072, China

(Received 20 January 2021; revised manuscript received 1 February 2021; accepted manuscript online 1 March 2021)

Grain boundary directed spinodal decomposition has a substantial effect on the microstructure evolution and properties of polycrystalline alloys. The morphological selection mechanism of spinodal decomposition at grain boundaries is a major challenge to reveal, and remains elusive so far. In this work, the effect of grain boundaries on spinodal decomposition is investigated by using the phase-field model. The simulation results indicate that the spinodal morphology at the grain boundary is anisotropic bicontinuous microstructures different from the isotropic continuous microstructures of spinodal decomposition in the bulk phase. Moreover, at grain boundaries with higher energy, the decomposed phases are alternating α/β layers that are parallel to the grain boundary. On the contrary, alternating α/β layers are perpendicular to the grain boundary.

Keywords: spinodal decomposition, grain boundary, phase-field method, pattern formation

PACS: 81.30.–t, 64.75.Nx, 68.35.Rh **DOI:** 10.1088/1674-1056/abea9b

1. Introduction

Spinodal decomposition is a common phase transition process in metallurgic alloys, oxide ceramics, colloidal gels, biominerals, *etc*.[1–5] It is governed by the competition between the destabilizing chemical free energy and the stabilizing composition gradient energy, which often results in the formation of domain structures with distinct chemical compositions. Cahn and Hilliard[6] proposed the fundamental theory for understanding the kinetic process of spinodal decomposition of bulk materials. As the periodic microstructures, developed during spinodal decomposition, crucially affect the properties of materials, the pattern-forming mechanisms and kinetic mechanisms associated with spinodal decomposition in immiscible mixtures have been studied widely in the last decades.[3,4,7–9]

As is well known, the properties of grain boundaries are very different from those of the grain interior, and the phase transition behavior at grain boundaries has been a perennial topic in materials and surface sciences for a century. In recent years, many investigations[9–12] indicated that grain boundary directed spinodal decomposition plays a crucial role in phase transitions. And the kinetics and pattern-forming mechanisms of grain boundary spinodal decomposition has attracted much attention, however, the effect of grain boundaries on spinodal decomposition is still unrevealed. Razumov's investigation results indicated that spinodal decomposition might be suppressed by the grain boundary for dilute solid solutions.[13] Conversely, Rajeshwari *et al*., Li *et al*., and Grönhagen *et al*.[10,12,14] reported that spinodal decomposition often starts earlier near defects or grain boundaries, which is mainly due to the fact that the atom diffusion is faster in these regions. Furthermore, the microstructure of spinodal decomposition will become more complicated due to the existence of interfaces. Liu *et al*.[15] found that the pattern of decomposed phases at high angle grain boundaries is alternating layers parallel to the grain boundary. The simulation and experimental results given by Li *et al*.[2,12,16] showed that the phase decomposition often begins at the grain boundaries, and then extends into the entire grain along the direction perpendicular to the grain boundary. Rajeshwari *et al*.[10] found that the morphology of precipitates at the grain boundary is related to the microstructure of grain boundaries. Tang and Karma,[17] and Wise *et al*.[17,18] investigated the surface-direct spinodal decomposition processes in thin-film materials, and proposed that the spinodal microstructure depends strongly on the magnitude of compositional strain and the thickness of the film.

As the spinodal decomposition is usually too fast to be captured in experiment, numerical simulation has become a powerful tool for studying the phase transition and spinodal decomposition.[19–26] In this work, a phase-field model of polycrystalline alloys, built by Ramanarayan and Abinandanan,[27] was used to study the grain boundary di-

*Project supported by the National Natural Science Foundation of China (Grant No. 51801154), the Fund from the State Key Laboratory of Solidification Processing in Northwestern Polytechnical University, China (Grant No. SKLSP201813), and the Shaanxi Provincial Science Fund for Distinguished Young Scholars, China (Grant No. 2018JC-027).

†Corresponding author. E-mail: cguo@xaut.edu.cn

© 2021 Chinese Physical Society and IOP Publishing Ltd

rected spinodal decomposition problem. The effect of grain boundary energy and concentration gradient energy on the spinodal decomposition were discussed in detail. And a pattern diagram of grain boundary directed spinodal decomposition as a function of gradient energy parameters was constructed. The present results can not only expand our knowledge of spinodal decomposition with the existence of grain boundaries but also provide guidance in designing the materials by the integration of the role at internal interfaces.

2. Phase-field model

The total free energy of the polycrystalline alloy phase-field model is written as[27]

$$F = \int \mathrm{d}V \left\{ f(c,\eta_i) + k_c (\nabla c)^2 + \sum_i k_\eta (\nabla \eta_i)^2 \right\}, \quad (1)$$

where c is the concentration field, η_i is the orientational order parameter to describe the grain i, $f(c,\eta_i)$ is the bulk free energy per unit, the second term and third term on the right-hand side represent the concentration gradient energy and grain boundary energy,[28] respectively. Here, $f(c,\eta_i)$ is[27]

$$f(c,\eta_i) = Ac^2(1-c)^2 + m(c) \times \left[0.25 + \sum_i \left(\frac{\eta_i^4}{4} - \frac{\eta_i^2}{2} \right) + \varepsilon \sum_i \sum_{j>i} \eta_i^2 \eta_j^2 \right], \quad (2)$$

where A and ε are constants, $m(c)$ is a composition-dependent function that couples the concentration field with the orientational order parameter field, and expressed as $m(c) = 1 + 0.5c^2 - 2.5c^2(1-c)^2$.

The evolution of the concentration field c is governed by the Cahn–Hilliard equation

$$\frac{\partial c(r,t)}{\partial t} = M\nabla^2 \frac{\partial F}{\partial c}, \quad (3)$$

where M is the atomic mobility, which is defined as[27]

$$M = M_\mathrm{b} + \varphi_\mathrm{g} M_\mathrm{t}, \quad (4)$$

where $M_\mathrm{b} = 1$, $M_\mathrm{t} = 1000$, and $\varphi_\mathrm{g} = [\sum_i \sum_{j>i} \eta_i^2 \eta_j^2]^{1/2}$. As the factor $\varphi_\mathrm{g} = [\sum_i \sum_{j>i} \eta_i^2 \eta_j^2]^{1/2}$ equals 1 inside the grain boundary and zero outside the grain boundary, the atom mobility at the grain boundary is much higher than that of the grain interior.

The evolution of the order parameter field η_i is governed by the Allen–Cahn equation

$$\frac{\partial \eta_i(r,t)}{\partial t} = -L \frac{\partial F}{\partial \eta_i}\Big|, \quad i = 1,2,3,\ldots,n, \quad (5)$$

where $L = 1000$ is a constant relaxation coefficient.

The dynamic equations above were solved by an open-source parallel finite element framework (MOOSE).[29] All the simulations were performed in a two-dimensional rectangle region of $L_x \times M_y = 128\Delta x \times 64\Delta y$ with periodic boundary conditions, where $\Delta x = \Delta y = 1$ and $\Delta t = 0.1$. Moreover, as all the parameters in this model were dimensionless, none of the simulation results correspond to a specific material.

3. Results and discussion

Figure 1 shows the microstructure evolution of the spinodal decomposition processes with different concentration gradient coefficients (kc): $kc = 0.1$, 0.5, 0.7, 0.9, and 2.0, where α phase is colored in blue and β phase is colored in red. The solid black line in Fig. 1(a) is the grain boundary. It is clear that the phase decomposition always originates from the grain boundary, and then extends into the grain interior, which is consistent with the simulation and experimental results of Li *et al.*[2,10,12,16] The absence of spinodal decomposition in the grain interior at the initial stage is due to the limited bulk diffusion.

For $kc = 0.1$, as shown in Fig. 1(a), that the spinodal decomposition morphology is dependent on simulation region. In the regions near the grain boundary, the interaction with solute atoms, resulting in the segregation of one phase from the grain boundary, which further results in the formation of the alternating α and β layers that parallel to the grain boundary. The phase decomposition process caused by such a kind of grain boundary segregation is named P-SD. While, for the regions far from the grain boundary, the random composition fluctuations grow to form the isotropic interconnected microstructures, just like general bulk spinodal decomposition (abbreviate to B-SD). As the atom diffusion is easier to happen at the grain boundary, P-SD is faster than B-SD. When the phase decomposition is completed, the final morphology is a combination of P-SD near the grain boundary and B-SD in the grain interior. With the increase of kc, the morphology of the decomposed phase will be changed significantly. For $kc \geq 0.9$, as shown in Figs. 1(d) and 1(e), the spinodal decomposition also begins at the grain boundary, which is consistent with the results in Fig. 1(a). The orientation of the alternating α and β primary phases is normal to the grain boundary, and then extends into the grain interior continually; finally, the simulation region will thoroughly be occupied by alternating α and β lamellas normal to the grain boundary, this kind of spinodal decomposition is N-SD. As for $0.5 \leq kc \leq 0.9$, the spinodal pattern near the grain boundary is a mixture between P-SD and N-SD. With the increase of kc, the volume fraction of N-SD at the grain boundary increases, while the volume fraction of B-SD in the grain interior decreases, the simulation results are shown in Figs. 1(b) and 1(c).

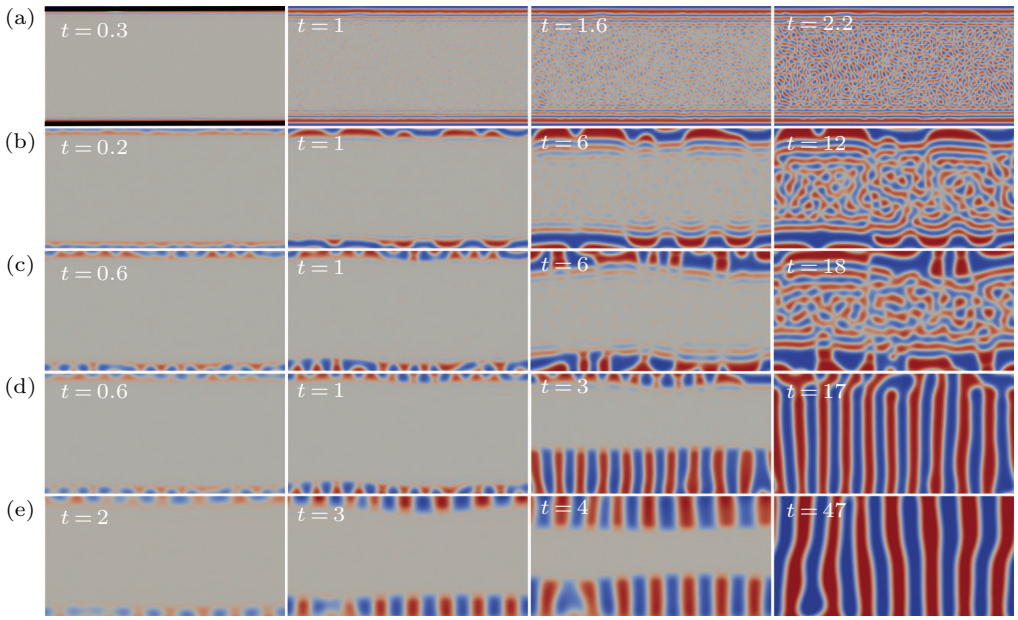


Fig. 1. Illustration of spinodal decomposition process with concentration gradient coefficient $kc = 0.1$ (a) 0.5 (b), 0.7 (c), 0.9 (d), and 2 (e), with solid black line denoting grain boundary in panel (a).

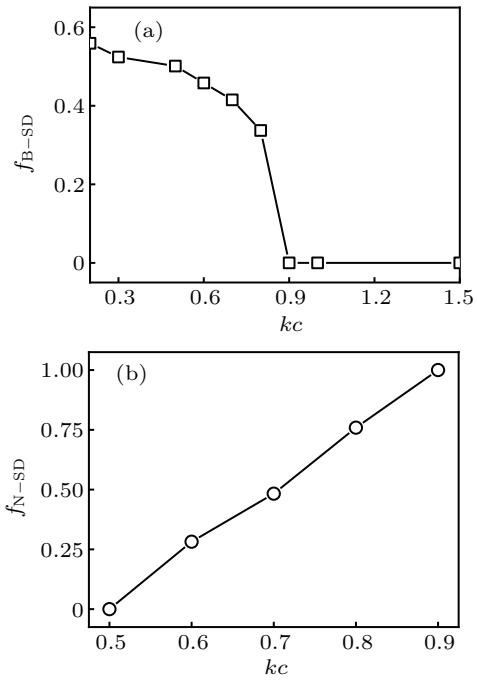


Fig. 2. (a) Volume fraction of bulk spinodal decomposition f_{B-SD} *versus* kc, and (b) volume fraction of grain-boundary-directed spinodal decomposition (normal to grain boundary f_{N-SD}) *versus* kc.

Comparing the results in Fig. 1, we know that the concentration gradient energy can significantly affect the shape of precipitation phas, and it is lath-shaped when kc is larger than 0.9 and irregularly shaped when kc is in a range of 0.5–0.7. Li *et al.*[30] obtained similar conclusions in Cu–Ni–Cr spinodal alloys. To figure out the influence of the concentration gradient term on the pattern formation of spinodal decomposition, volume fractions of different spinodal structures *versus* kc are summarized in Fig. 2 quantitatively. From Fig. 2(a), the volume fraction of B-SD (f_{B-SD}) decreases continually with kc increasing, and $f_{B-SD} = 0$ for $kc > 0.9$. This phenomenon mainly due to the concentration gradient energy suppressing the growth of random fluctuation domains in the interior of the grain, which further leads the grain boundary directed spinodal decomposition to overcome the B-SD under some conditions, such as the simulation results in Figs. 1(d) and 1(e). Figure 2(b) shows the variation of f_{N-SD} (the volume fraction of N-SD near the grain boundary) with kc. It is clear that $f_{N-SD} = 0$ for kc less than 0.5 and $f_{N-SD} = 1$ for kc larger than 0.9, while for kc between 0.5 and 0.9, f_{N-SD} increases continuously with kc increasing. We believe that this is due to the fact that the N-SD is more favorable in energy than P-SD for a larger kc, which will be discussed later.

Figure 3 shows the microstructure evolution processes with different values of grain boundary energy coefficient $k\eta$, from which the influence of grain boundary on spinodal decomposition can be further understood. The phase decomposition also occurs initially at the grain boundary, which is consistent with the above simulation results. From Fig. 3, we can see that the spinodal decomposition is N-SD-dominated for $k\eta \leq 1$, while it will be P-SD-dominated for $k\eta \geq 4$. As for $k\eta$ between 1 and 4, the final morphology of decomposed phases is a mixture between P-SD and N-SD, and the volume fraction of N-SD decreases with $k\eta$ increasing. Previous results of Li *et al.*[2] verified that the phase decomposition at low angle tilt grain boundaries was P-SDlike. Yang *et al.*[31] investigated the spinodal decomposition process with different grain boundary angles by an atomic method and reported that the ultimate pattern of the decomposed phases was P-SDlike for high angle grain boundaries.

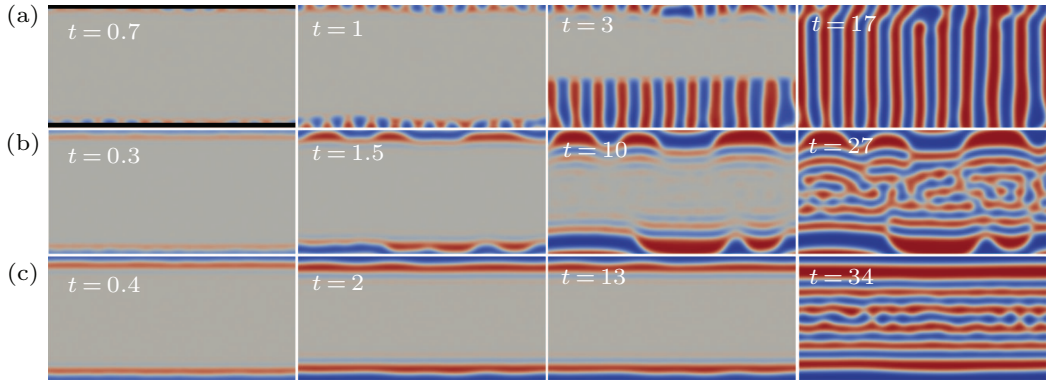


Fig. 3. Illustration of spinodal decomposition process with grain boundary energy coefficient $k\eta = 1$ (a), 2 (b), and 4 (c), with solid black line denoting grain boundary in panel (a).

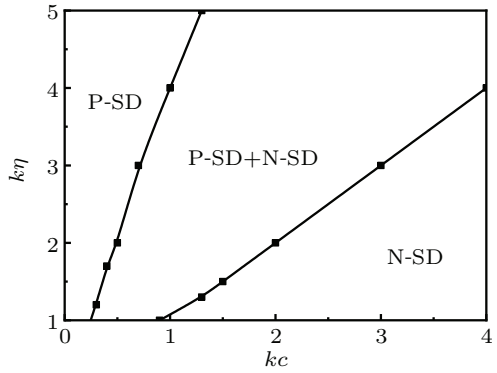


Fig. 4. Phase-diagram of spinodal morphology as a function of gradient energy coefficient, showing plots of $k\eta$ *versus* kc.

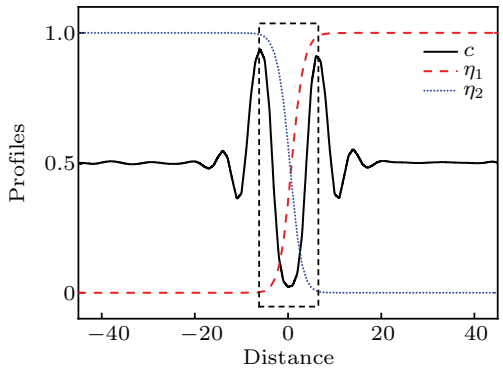


Fig. 5. Plots of c, η_1, and η_2 *versus* distance normal to grain boundary.

From the simulation results in Figs. 1 and 3, it is found that the spinodal decomposition pattern near the grain boundary can be influenced by concentration gradient energy and grain boundary energy. An interesting phenomenon is that the kc and $k\eta$ have similar effects on the spinodal morphology. To reveal the law of spinodal pattern selection, various grain boundary directed decomposition morphologies are summarized as a function of kc and $k\eta$, and shown in Fig. 4. We can see that the phase decomposition at the grain boundary is P-SDdominated in the region $k\eta \geq 4kc$, and the volume fraction of P-SD increases with $k\eta$ increasing. According to the classical phase-field model[32] and the kinetics analysis of the spinodal decomposition process,[33] the thickness of the grain boundary (w_g) is proportional to $\sqrt{k_\eta}$, while the critical wavelength (λ_{cri}) of spinodal decomposition is proportional to $2\sqrt{k_c}$. Therefore, the critical line for P-SD can also be treated as $w_g \geq \lambda_{cri}$, which is consistent with the distribution of c and η in Fig. 5. This is mainly due to the fact that when $w_g \geq \lambda_{cri}$ the wavelength of the concentration field reaches the critical value λ_{cri} more easily under the effect of solute segregation along the grain boundary, which further results in P-SD. Such a kind of segregation-driven grain boundary spinodal decomposition has been reported as a crucial phase transition mechanism in high-entropy alloy recently.[12]

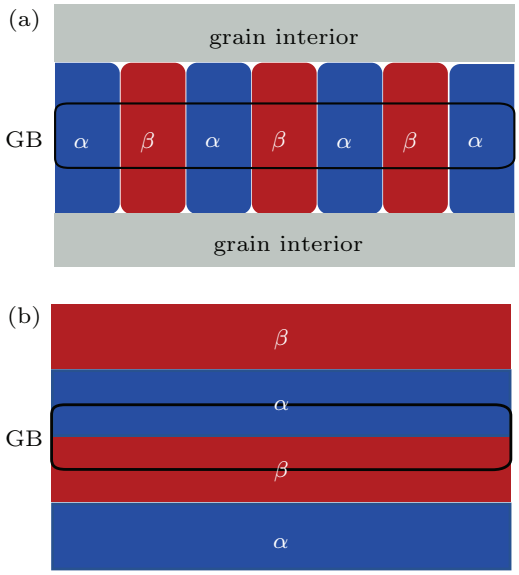


Fig. 6. (a) Schematic diagram of simulated positional relationship between grain boundary and alternating α/β lamellas for N-SD, and (b) schematic diagram of alternating α/β lamellas parallel to grain boundary. The region inside the black box is the grain boundary (GB).

To ascertain the reason why the pattern formation is N-SD-dominated for $k\eta \leq kc$, we further analyze the energy difference between the two spinodal decomposition mechanisms of the initial stages. Schematic diagrams indicating the positional relationship between the grain boundary and the alternating α/β lamellas for $k\eta = kc$ are shown in Fig. 6, where the lamellae are perpendicular to the grain boundary in Fig. 6(a)

and parallel to the grain boundary in Fig. 6(b). Owing to the fast diffusion and segregation effects of grain boundaries, the spinodal decomposition in grain boundaries can finish in an instant. Hence, the interfacial energy and width of the grain boundary and α/β phase boundary can be obtained conveniently. Then the energy difference ΔF between N-SD and P-SD inside the black box as shown in Fig. 6 can be obtained as follows:

$$\Delta F = \frac{L\sqrt{k\eta}}{\sqrt{kc}}\gamma_{\mathrm{m}} - L\gamma_{\mathrm{m}} = L\gamma_{\mathrm{m}}\left(\frac{\sqrt{k\eta}}{\sqrt{kc}} - 1\right), \tag{6}$$

where γ_{m} is the phase boundary energy between α and β, and L is the length of the grain boundary. According to Eq. (6), it is clear that the N-SD is more favorable in energy for $k\eta \leq kc$, which is consistent with the above simulation result.

4. Conclusions

In this work, the morphological evolution of grain boundary directed spinodal decomposition is studied by the phase-field model. Owing to the effect of interaction between the grain boundary with solute atoms and the grain boundary diffusion being faster than bulk diffusion, the phase decomposition at the grain boundary always occurs faster than in other regions. Unlike the case of spinodal decomposition with isotropic continuous microstructures in the bulk phase, the spinodal morphology at the grain boundary is of the anisotropic bicontinuous microstructure. Three different kinds of spinodal morphologies near the grain boundary are found in our simulations: lath-shaped decomposed phases parallel to the grain boundary, P-SD; lath-shaped decomposed phases normal to the grain boundary, N-SD; irregularly shaped spinodal morphology, *i.e.*, a mixture between P-SD and N-SD. The morphology of grain boundary directed spinodal decomposition can be dependent on the ratio between the concentration gradient energy coefficient kc and the grain boundary energy coefficient $k\eta$. For $k\eta \geq 4kc$ the phase decomposition will be P-SD-dominated, while N-SD is more favorable in energy for $k\eta \leq kc$. As for $4kc \leq k\eta \leq kc$, spinodal morphology will be a mixture between P-SD and N-SD. These findings can expand our knowledge of the grain boundary directed spinodal decomposition and help to provide guidance in designing novel materials.

References

[1] Moore K T, Johnson W C, Howe J M, Aaronson H I and Veblen D R 2002 *Acta Mater.* **50** 943
[2] Li Y S, Li S M and Zhang T 2009 *J. Nucl. Mater.* **395** 120
[3] Zhou L, Guo W, Poplawsky J D, Ke L, Tang W, Anderson I E and Kramer M J 2018 *Acta Mater.* **153** 15
[4] Seknazi E, Kozachkevich S, Polishchuk I, Bianco Stein N, Villanova J, Suuronen J P, Dejoie C, Zaslansky P, Katsman A and Pokroy B 2019 *Nat. Commun.* **10** 4559
[5] Guo C, Wang J, Li J, Wang Z, Huang Y, Gu J and Lin X 2018 *Acta Mater.* **145** 175
[6] Cahn J W and Hilliard J E 1958 *J. Chem. Phys.* **28** 258
[7] Radnóczi G, Bokányi E, Erdélyi Z and Misják F 2017 *Acta Mater.* **123** 82
[8] Kwiatkowski da Silva A, Ponge D, Peng Z, Inden G, Lu Y, Breen A, Gault B and Raabe D 2018 *Nat. Commun.* **9** 1137
[9] Lach T G, Frazier W E, Wang J, Devaraj A and Byun T S 2020 *Acta Mater.* **196** 456
[10] Rajeshwari K S, Sankaran S, Hari Kumar K C, Rösner H, Peterlechner M, Esin V A, Divinski S and Wilde G 2020 *Acta Mater.* **195** 501
[11] Kwiatkowski da Silva A, Kamachali R D, Ponge D, Gault B, Neugebauer J and Raabe D 2019 *Acta Mater.* **168** 109
[12] Li L, Li Z, Kwiatkowski da Silva A, Peng Z, Zhao H, Gault B and Raabe D 2019 *Acta Mater.* **178** 1
[13] Razumov I K 2018 *Russ. J. Phys. Chem. A* **92** 1338
[14] Grönhagen K, Ågren J and Odén M 2015 *Scr. Mater.* **95** 42
[15] Liu J, Wu X, Lennard W N, Landheer D and Dharma-Wardana M W C 2010 *J. Appl. Phys.* **107** 123510
[16] Li Y, Katsui H and Goto T 2017 *Mater. Today: Proceedings* **4** 11449
[17] Tang M and Karma A 2012 *Phys. Rev. Lett.* **108** 265701
[18] Wise S M, Kim J S and Johnson W C 2005 *Thin Solid Films* **473** 151
[19] Hu S Y and Chen L Q 2004 *Acta Mater.* **52** 3069
[20] Seol D J, Hu S Y, Li Y L, Shen J, Oh K H and Chen L Q 2003 *Acta Mater.* **51** 5173
[21] Steyn-Ross M L, Steyn-Ross DA, Voss L J and Sleigh J W 2019 *Phys. Rev. E* **99** 012318
[22] Lee J and Chang K 2019 *Comput. Mater. Sci.* **169** 109088
[23] Sun J, Li X, Zhang J, Wang G, Yang M, Wang H and Xu D 2020 *Acta Metall. Sin.* **56** 1113
[24] Qi K W, Zhang Y H, Guo H J, Tian X L and Hou H 2019 *Acta Phys. Sin.* **68** 170504 (in Chinese)
[25] Song Y H, Wang M T, Ni J, Jin J F and Zong Y P 2020 *Chin. Phys. B* **29** 128201
[26] Zhang Z D, Cao Y T, Sun D K, Xing H, Wang J C and Ni Z H 2020 *Chin. Phys. B* **29** 028103
[27] Ramanarayan H and Abinandanan T A 2004 *Acta Mater.* **52** 921
[28] Guo C, Wang J, Wang Z, Li J, Guo Y and Huang Y 2016 *Soft Matter* **12** 4666
[29] Tonks M R, Gaston D, Millett P C, Andrs D and Talbot P 2012 *Comput. Mater. Sci.* **51** 20
[30] Li X N, Li Z M, Cheng X T, Sun W, Zheng Y H, Yu Q X, Wang C Y, Wang Q and Dong C 2019 *Mater. Chem. Phys.* **223** 486
[31] Yang T, Chen Z, Zhang J, Dong W P and Wu L 2012 *Chin. Phys. Lett.* **29** 1
[32] Schwalbach E J, Warren J A, Wu K A and Voorhees P W 2013 *Phys. Rev. E* **88** 023306
[33] Guo Z 2019 *Kinetics and Crystallography of Solid State Transformation* (Shanghai: Shanghai Jiao Tong University Press) pp. 83–88